Journal of Materials Chemistry A

Accepted Manuscript

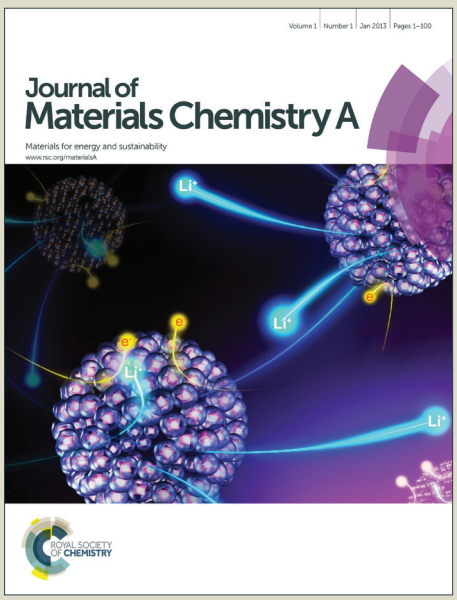

ROYAL SOCIETY OF CHEMISTRY

www.rsc.org/materialsA

Pr Nathalie Steunou

Institut Lavoisier (UMR CNRS 8180)

Université de Versailles-Saint-Quentin-en-Yvelines (UVSQ)

45 avenue des Etats Unis 78035 Versailles cedex

FRANCE

Tel : 33 1 39 25 43 73

Fax: 33 1 39 25 44 52

e-mail :nathalie.steunou@uvsq.fr

Keywords: polyoxometalate, gelatin, coacervation, sensors, modified electrode

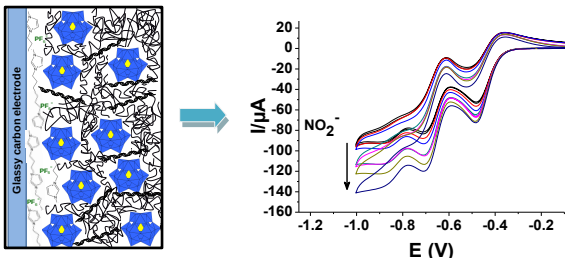

Novel modified electrodes prepared by a layer-by-layer deposition of polyoxotungstate and gelatin solutions exhibit excellent electrocatalytic performance for nitrite detection.

Table of contents entry

Steunou et al

Interfacing an heteropolytungstate complex and gelatin through a coacervation process: design of bionanocomposite films as novel electrocatalyst.†

Basma Khadro,[a] Imane Baroudi,[a] Anne-Marie Goncalves,[a] Bruno Berini,[b] Bruce Pegot,[a] Farid Nouar,[a] Thi Ngoc Ha Le,[a] François Ribot,[c1-3] Christel Gervais,[c1-3] Florent Carn,[d] Emmanuel Cadot,[a] Christine Mousty,[e] Corine Simonnet-Jégat,[a] Nathalie Steunou.[*,a]

Bionanocomposite films on glassy carbon electrode (GCE) have been prepared by a very straightforward and reliable method based on a layer-by-layer deposition of polyoxometalate (POM) (i. e. $[BW_{12}O_{40}]^{5-}$) and gelatin solutions. The strong immobilisation of $[BW_{12}O_{40}]^{5-}$ at the surface of the GCE results from electrostatic interactions between gelatin and POM, as evidenced in a hybrid hydrogel prepared by a coacervation process. The GCE has also been modified by imidazolium based ionic liquids in order to increase the charge transfer rate. Two modified electrodes with one or two POM layers have been prepared by this strategy. When compared to other POM-based modified electrodes, the novel electrodes with two POM layers exhibit excellent electrocatalytic performance for nitrite detection at pH 3 in terms of sensitivity (868 $mA.M^{-1}.cm^{-2}$) and linear range of nitrite concentrations (50-600 μM).

[a] *Institut Lavoisier de Versailles, UMR CNRS 8180, UVSQ, 45 avenue des Etats-Unis 78035 Versailles Cedex. France. E-mail: nathalie.steunou@uvsq.fr Fax: +33 1 39 25 43 73 ; Tel : +33 1 39 25 44 52.*
[b] *Groupe d'Etude de la Matière Condensée, UMR CNRS 8635, 45 avenue des Etats-Unis 78035 Versailles Cedex.*
[c1] *Sorbonne Universités, UPMC Univ Paris 06, UMR 7574, Chimie de la Matière Condensée de Paris, F-75005, Paris, France,* [c2] *CNRS, UMR 7574, Chimie de la Matière Condensée de Paris, F-75005, Paris, France.* [c3] *Collège de France, UMR 7574, Chimie de la Matière Condensée de Paris, F-75005, Paris, France.*
[d] *Laboratoire Matière et Systèmes Complexes (MSC), UMR CNRS 7057, Université Paris Diderot, Bât. Condorcet, 10 rue A. Domon et L. Duquet, 75013 Paris, France.*
[e] *Institut de Chimie de Clermont-Ferrand ICCF, CNRS UMR 6296, Université Blaise Pascal 63171 Aubière Cedex, France.*
† Electronic supplementary information (ESI) available : FT-IR peaks of $[BW_{12}O_{40}]^{5-}$-gelatin hybrids, ^{11}B NMR spectra of $[BW_{12}O_{40}]^{5-}$, QELS, CVs of GCE, ILGCE, $[BW_{12}]$-ILGCE and $[BW_{12}]$-G-ILGCE, CV of 2$[BW_{12}]$-G-ILGCE prepared from different gelatin solutions (1, 2, 3 wt%), SEM images of gelatin and 2[BW12]-G-IL coatings and elemental mapping by EDX.

1. Introduction

A tremendous effort has been devoted during the past decades to the production of a wide range of inorganic or hybrid nanomaterials with different potential applications in energy, medicine, and environment domains.[1] Furthermore, due to the emerging energy resource crisis and ecological concerns, the next challenging and logical step towards the production of nanodevices is to significantly reduce the necessary amount of functional materials and process nanomaterials with a "green technology" using low-cost and environment friendly synthesis procedures (precursors and solvent of low toxicity).[2]

Bionanocomposites represent an emerging class of materials derived from natural polymers and inorganic solids interacting at the nanometre scale.[3] The main advantage of using macromolecules of natural origin is related to their chemical complexity and self-assembly properties, for which no synthetic equivalent is usually available, together with their sustainable character namely their large abundance and non-fossil origin, two key aspects for the development of "green" materials. Among biopolymers, gelatin is widely used in food, pharmaceutical industries due to its ability to form transparent and elastic gels.[4] This protein obtained by hydrolytic degradation of mammalian or fish collagen[5] is soluble in water above the temperature of gelification (T_{gel}, which is close to 27 °C for a mammalian gelatin) while it forms reversible physical gels below T_{gel} due to the partial recovering of the triple-helix conformation of the native collagen. In the field of materials science, thin films or hybrid particles with optical, photochromic or sensing properties have been synthesised through the homogeneous dispersion or encapsulation of different inorganic solids including calcium phosphate, hydroxyapatite, clay minerals, silica, layered perovskites or metallic nanoparticles into transparent gelatin matrices.[6,7] In those materials, the texturation of the materials as well as the distribution and size of inorganic nanoparticles are controlled by the complexation driven assembly of inorganic precursors and gelatin.[6,7]

Polyoxometalates (POMs) are discrete, molecularly defined inorganic metal oxide clusters with dimensions ranging from approximately one to several nanometres.[8] Their architectures not only exhibit a wide variety of topologies and compositions, but also lead to chemical, physical, and electronic versatility. To date, the assembly of polyoxometalates and oppositely charged polyelectrolytes (polyamines, polyampholyte copolymer, surfactants, gelatin etc…) through electrostatic interactions can be an attractive strategy to prepare tunable well-defined organic-inorganic supramolecular architectures with potential applications in catalysis, magnetism, electro- and photochromism and so on.[9,10,11] Recently, this approach has also been used as an encapsulation tool of pharmacologically active POMs for the design of drug delivery systems.[12] The interest devoted to POMs for the elaboration of hybrid materials is related to their interesting and unique molecular, structural (i. e., thermal and redox stability, nanoscopic topology, good solubility, strong acidity…) electronic and magnetic properties.8,[13] In particular, POMs have the ability to proceed without alteration of their structure in multiple, consecutive and reversible multielectron charge transfer reactions which are the basis for many catalysis processes.8 During the past few years, several approaches for the modification of electrodes by POMs have been reported aiming at improving the analytical performance of electrochemical sensors and their poor long-term stability. They include various deposition methods such as electrochemical,[14] layer-by-layer,[14b,15,16] strategies as well as the entrapment in sol-gel[17,18], polymeric[19], biopolymeric[20], carbon nanotubes[21,22] or graphene[23] matrices. Very recently, POMs-modified electrodes have been built by combining POMs with organic dyes that serve as electron mediator.[24] A promising nitrite sensor based on one-dimensional POM hybrid nanofibres has also been recently developed by an electrospinning process.[25] Despite of the fact that most of these electrodes present interesting electrochemical properties, their multi-steps construction is generally complicated involving the incorporation of a high number of species. Moreover, most of the POMs-modified

electrodes reported so far can only operate in strong acidic aqueous solutions (pH ~1) due to the weak stability of most POMs in neutral or alkaline aqueous solutions which limits their potential for practical application. Therefore, the research for simple and reliable methods to immobilise and stabilize POMs on electrodes still remains a challenge.

Recently, we have reported that electrostatic attractive interactions between a polyoxometalate (i. e. the decavanadate, $[H_2V_{10}O_{28}]^{4-}$) and positively charged gelatin chains [26,27] could induce a two-step liquid-liquid phase separation process fully consistent with a complex coacervation behaviour.[28] Such process mainly reported for proteins and organic polyelectrolytes of opposite charges[29] is currently used as a micro-encapsulation tool[30] in pharmacy, cosmetics and food industry or as a method for protein purification.[31] It implies the formation of weakly-charged colloidal aggregates that rearrange in solution and condense into a micro-gel phase upon increasing polyelectrolyte concentration. We have particularly investigated the influence of decavanadate clusters on the thermo-reversible gelation of gelatin solution by combining rheology and micro-calorimetry, showing the complex and non-fully reversible behaviour of rheological properties of the decavanadate / gelatin system with temperature.[27] In contrast to temperatures higher than 30°C where the decavanadates can act as physical cross-linkers, the elastic properties of gelatin are only slightly enhanced by the presence of decavanadates at room temperature and mainly governed by the concentration of gelatin triple helices.[27] The supramolecular organization of the gelatin matrix which can be controlled by the pH and temperature conditions has also been used to direct the organization of the decavanadates or the nucleation/growth of V_2O_5 nanoribbons that presumably bind to the positively charged lysine residues of gelatin.[7] By this approach, it was possible to design a well-defined decavanadate-gelatin material which exhibits a striking rubber-like behaviour and enhanced mechanical properties than pure gelatin hydrogels.[7]

In the present work, the coacervation process with gelatin has been extended to a Keggin-heteropolytungstate $[BW_{12}O_{40}]^{5-}$ whose electrochemical characterization of a single crystal has been recently reported.[32] This study shows that crystals of $[BW_{12}O_{40}]^{5-}$ are characterized by a large population of redox sites and mobile protons, and a high effective diffusion coefficient for mass transfer, both requirements for the development of solid state electrochemical devices.

In our present work, the first step was to determine the physical-chemical conditions (pH, temperature, POM and gelatin concentrations) that may induce the formation of $[BW_{12}O_{40}]^{5-}$-gelatin coacervates while preserving the molecular structure of $[BW_{12}O_{40}]^{5-}$. Then, $[BW_{12}O_{40}]^{5-}$-gelatin bionanocomposite films have been processed on glassy carbon electrode (GCE) through a simple layer-by-layer deposition method. The GCE has also been modified by imidazolium based ionic liquids (ILs) before casting the $[BW_{12}O_{40}]^{5-}$-gelatin hydrogels. Indeed, recent works on modified electrodes have taken advantage of the electrochemical and physical-chemical properties of ILs (high ionic conductivity, wide electrochemical window, high chemical and thermal stability, negligible vapour pressure) and shown that POMs exhibit improved electrochemical sensitivity when associated to ILs.[33,34,35,36,37] In the last part of this study, the electrochemical properties of the 2$[BW_{12}]$-gelatin-IL-GCE electrodes and their electrocatalytic activity towards the reduction of nitrite have been studied. In particular, these modified electrodes present excellent analytical performances for the titration of nitrites at pH 3 in terms of sensitivity and linear concentration range. In this context, the development of efficient, simple and low cost sensors for nitrites determination is particularly important due to the environmental impact of this pollutant in water sources as a consequence of the widespread use of fertilizers. Moreover, as food preservative, nitrite is also present in waters, foods and beverages. However, due to its high toxicity, the European Community has recommended that the nitrite level should never exceed 0.1 $mg.L^{-1}$ (~2.2 mM) in drinking

water.[22,38] Therefore, the concentration of nitrite in beverages and foods is a societal issue for human health.

2. Experimental Section

2. 1 Chemicals.

Commercial gelatin extracted from porcine skin (type A with a bloom of ~175 g) corresponding to an average molecular weight of ~ 40000 $g.mol^{-1}$ and an isoelectric point (I.E.P) close to 8 (according to the supplier) was purchased from Sigma-Aldrich.

2.2 Synthesis of $K_5[BW_{12}O_{40}].11H_2O$.

The compound $K_5[BW_{12}O_{40}].11H_2O$ has been synthesised according to the procedure reported by Rocchiccioli-Deltcheff *et al*.[39] The structure of the polyoxometalate $[BW_{12}O_{40}]^{5-}$ is shown in scheme 1b). The potassium salt $K_5[BW_{12}O_{40}].11H_2O$ has been characterised by combining FT-IR and ^{11}B MAS NMR spectroscopies (see Fig. 1). The stability of $[BW_{12}O_{40}]^{5-}$ at concentrations between 10^{-2} and 2.10^{-4} M and pH=3 has been studied. After dissolution of the potassium salt $K_5[BW_{12}O_{40}].11H_2O$ in aqueous solution, the initial pH close to 5.6 is lowered to 3 by adding small volumes of 0.1 M HCl solution. The resulting solutions of $[BW_{12}O_{40}]^{5-}$ at pH=3 are characterised by combining solution ^{11}B NMR spectroscopy and cyclic voltammetry (Fig.S1 of ESI and Fig. 2(a)).

2.3 Preparation of gelatin solutions.

Gelatin solutions were prepared by swelling the gelatin granules in an aqueous solution during a minimum of 3 h at 5 °C. Gelatin was then dissolved at 45 °C using a magnetic stirrer for 30 min at 300 rpm.

2.4 Preparation of $[BW_{12}O_{40}]^{5-}$- gelatin mixtures

When a 4 wt% (~1 mM) gelatin solution is prepared, its pH is adjusted to pH=3 with an aqueous HCl solution (2 M) and the temperature fixed at 40 °C. Aqueous solutions of $[BW_{12}O_{40}]^{5-}$ of different concentrations are also prepared at pH 3 and 40°C. Then a volume of the aqueous $[BW_{12}O_{40}]^{5-}$ solution and a volume of the gelatin solution are mixed and stirred during 20 min at 300 rpm and 40 °C. At low $[BW_{12}O_{40}]^{5-}$ concentrations (i. e. c≤0.3 mM), homogeneous transparent white solutions are obtained while at higher $[BW_{12}O_{40}]^{5-}$ concentrations (i.e. c> 0.7 mM), biphasic samples composed of a dense viscous white phase below a transparent solution are prepared. At intermediate $[BW_{12}O_{40}]^{5-}$ concentrations, turbid white solutions are immediately obtained that turn to biphasic samples upon ageing (Fig.3).

2.5 Synthesis and characterisation of ionic liquids [bmim][X].

The ionic liquids [bmim] [X] (with X^- = Cl^-, Br^-, PF_6^-, OTf^-, BF_4^-) (see scheme 2) have been prepared according to earlier publication.[40] The general synthesis of imidazolium based ionic liquids involves a consecutive quaternisation-anion metathesis procedure. The first step leads to an alkylated halide precursor ([bmim] [Br] and [bmim] [Cl]). The second step involves an anion exchange of azolium halides with an alkaline earth metal or ammonium salts of charge-delocalized soft anion (BF_4^-, PF_6^-, OTf^-). They were characterised by ^1H and ^{13}C solution NMR spectroscopies on Bruker Avance 200 and 300 MHz spectrometers in chloroform-d or acetone-d6 with the residual peak solvent as an internal standard. ^{19}F NMR spectra were acquired on a Bruker Avance 200 MHz spectrometer. The chemical shifts were measured relative to the internal standard $CFCl_3$ (δ= 0 ppm). The complete characterisation of these ILs is in full agreement with literature.[41]

2.6 Characterisation. Infrared spectra were recorded on a FTIR Magna 550 Nicolet spectrophotometer using the technique of pressed KBr pellets at a resolution of 4 cm^{-1}.Quasi-elastic light scattering (QELS) measurements were performed on a Malvern Zetasizer Nano-ZS equipment with a 4 mW HeNe LASER operating at λ = 632.8 nm. The normalized time autocorrelation functions of the scattered intensity, g(2)(q,t), were measured at 173 °. The autocorrelation functions of the concentration fluctuations, g(1)(q,t) were derived from g(2)(q,t) through the Siegert relationship. g(1)(q,t) were then analysed through a cumulant analysis stopped at the second order for monomodal distributions and through Laplace Inversion by CONTIN algorithm for bimodal or highly polydisperse distributions. These measurements have been performed on diluted gelatin solution (1.5 wt%, ~0.375 mM) to minimise multiple scattering effects (Fig. S2 of ESI). Solution ^{11}B NMR was performed on a Bruker 300 Avance III spectrometer, operating at 96.3 MHz, equipped with a BBO 10 mm Bruker probe. The 90° pulse was 9.2 µs, the interpulse delay 20 s and the acquisition time 0.34 s. The experiments were performed without lock (field drift < 1 Hz/h). Chemical shifts were referenced using a secondary external reference, $B(O^iPr)_3$ in $CDCl_3$, at 17.5 ppm relatively to BF_3•OEt_2. Quartz NMR tubes were used to avoid the ^{11}B very broad signal (~0 ppm) arising from borosilicate glass tubes. Nevertheless, two very broad (FWHM ~5000Hz) and weak signals, due to the probe, could still be observed around 40 and -50 ppm for the most diluted samples. The resonances related to $[BW_{12}O_{40}]^{5-}$ being much narrower (FWHM < 200 Hz) and located between 20 and -5 ppm, they were easily differentiated from the probe signals. ^{11}B MAS NMR spectra were recorded at 11.75 T on a Bruker Avance 500 wide-bore spectrometer operating at 128.28 MHz, using a Bruker 4 mm probe and a spinning frequency of the rotor of 14 kHz. The spectra were acquired using a spin-echo θ-τ-2θ pulse sequence with θ = 90° to overcome problems of probe signal. The τ delay was synchronized with the spinning frequency and recycle delay of 1s was used. Chemical shifts were

referenced to $BF_3(OEt)_2$ (δ = 0 ppm). SEM images have been recorded on a JEOL JSM-7001F microscope using gold-coated samples equipped with an energy-dispersive X-ray (EDX) spectrometer with a X-Max SDD (Silicon Drift Detector) by Oxford. AFM images were recorded on a Bruker AXS equipment in tapping mode. Commercial tips (FESP-Bruker) with a weak spring constant (k=3N/m) and low resonant frequency (64 kHz) were used.

2.7 Electrochemical measurements

All cyclic voltammograms are carried out with a potentiostat Autolab connected to a thermostated cell with a three-electrode system. The working electrodes are glassy carbon electrodes (GCE) (diameter 3 mm). A Pt wire was used as counter electrode and all potentials were measured relative to an Ag/AgCl saturated KCl electrode. The electrolyte solutions (0.5 M Na_2SO_4 aqueous solution or 1M $CHCl_2COOH/CHCl_2COONa$ buffer solutions) were deaerated thoroughly for at least 30 min with pure argon and kept under a positive argon atmosphere during the experiments. For cyclic voltammograms of dissolved $[BW_{12}O_{40}]^{5-}$, the polishing of the glassy carbon (GC; Le Carbone Lorraine, France) electrodes has been performed as described earlier.[42] The uncertainty in the redox potential values as measured on different CVs recorded under these working conditions is evaluated to be equal to 4 mV.

2.8 Preparation of $[BW_{12}]$-G-modified Ionic Liquid Glassy Carbon electrode ($[BW_{12}]$-G-ILGCE)

For the preparation of modified electrodes by immobilisation of $[BW_{12}O_{40}]^{5-}$ (i. e. $[BW_{12}]$-G-ILGCE), the surface of the GCE is prepared by polishing with 6, 3 and 1 µm alumina powder and rinsed abundantly with ultra pure milliQ water, ethanol and acetone between two sequential polishing steps. These electrodes are then immersed in solutions of nitric acid and acetone (v:v=1/1) for one minute and then sonicated in ethanol solution for 15 min. Prior to

the experiment, the GCE is scanned by successive cyclic voltammetry within the potential range +0.6 to -1.0 V in the deoxygenated electrolyte solution (i. e. 0.5 M Na_2SO_4 aqueous solution) to obtain a clean surface. The $[BW_{12}]$-G-ILGCE is prepared as follows: the cleaned and well-dried GCE is immersed in a solution of ionic liquid during 2h. The electrochemical response of GCE modified by different imidazolium based ionic liquids [bmim] [X] (with X^- = PF_6^-, OTf^-, Cl^-, Br^-, BF_4^-) has been evaluated in 0.5 M Na_2SO_4 aqueous solution at pH=3 (see Fig. 4 and Fig. S3 of ESI). Since the current base line depends on the nature of the counter ions and is the highest with PF_6^-, the glassy carbon electrodes have been systematically modified with [bmim] $[PF_6]$. Solutions of $[BW_{12}O_{40}]^{5-}$ and gelatin are alternatively deposited at the surface of the ILGCE to permit the formation of layers of POM and gelatin. The $[BW_{12}]$-G-ILGCE (1 POM layer) is formed by casting first 10 µL of a 0.5 mM $[BW_{12}O_{40}]^{5-}$ and then 10 µL of 1 wt% gelatin solution (40°C) on the surface of the modified electrode. For the $2[BW_{12}]$-G-ILGCE (2 POM layers), a second POM layer is formed by dropping an additional 10 µL volume of a 0.5 mM POM solution onto the surface of $[BW_{12}]$-G-ILGCE. After deposition of each POM and gelatin layer, the modified electrodes are dried at room temperature for 30 min. The $[BW_{12}]$-G-ILGCE and $2[BW_{12}]$-G-ILGCE are then washed in ultra pure milliQ water in order to remove the POMs that are not immobilised by electrostatic interactions at the surface of the electrode. The electrochemical properties of both $[BW_{12}]$-G-ILGCE and $2[BW_{12}]$-G-ILGCE are compared to those of $[BW_{12}]$-ILGCE prepared by casting only the $[BW_{12}O_{40}]^{5-}$ solution (10 µL, 0.5 mM) on ILGCE (Fig. S4 of ESI). The impact of the gelatin concentration on the electrochemical properties of $2[BW_{12}]$-G-ILGCE has also been studied (Fig. S5(a) of ESI). For SEM-EDX and AFM experiments, $2[BW_{12}]$-gelatin coatings were deposited on diamond wafers (1 cm x 1 cm) (Fig. S6 of ESI). Two coatings have been prepared depending on the volume of solution deposited. First, 20 µL of a 0.5 mM $[BW_{12}O_{40}]^{5-}$ solution, then 20 µ L of a 1 wt% gelatin solution and finally 20 µ L

of a 0.5 mM $[BW_{12}O_{40}]^{5-}$ solution have been alternately cast on the surface of the diamond wafer. After deposition of each solution, the 2[BW_{12}]-G coatings are dried at room temperature for about 2h. A second coating has been prepared by the deposition of 10 µL of each solution. Both coatings have been rinsed with distilled water and dried at room temperature.

3. Results and discussion

3.1 Stability of $[BW_{12}O_{40}]^{5-}$ in conditions of low concentrations and pH=3.

In order to prepare bionanocomposites between gelatin and $[BW_{12}O_{40}]^{5-}$, the first step consists to determine a pH domain where both species are stable and may interact by electrostatic interactions. In acidic solution, gelatin macromolecules are in a random coil conformation with fully protonated amine (pKa NH_3^+/NH_2 ≈ 10.5) and carboxylic acid functions (pKa $COOH/COO^-$ ≈ 4) giving rise to a global positive charge (pI ≈ 8). Thus, gelatin behaves like a weak cationic polyelectrolyte below pH 8. Therefore, attractive electrostatic interactions between $[BW_{12}O_{40}]^{5-}$ and gelatin may be expected at pH<4. Our previous work on the coacervation process between $[H_2V_{10}O_{28}]^{4-}$ and gelatin has clearly shown the suppression of any interactions at pH≥4.5, which is certainly due to the deprotonation of carboxylic acid functions of gelatin and thus to a decrease of the global positive charge of gelatin.[26] Moreover, as polyoxometalates are labile molecular clusters that are sensitive towards hydrolysis especially in diluted aqueous solutions, it was of primary importance to ascertain that $[BW_{12}O_{40}]^{5-}$ is stable at low concentration (typically 0.5 mM) and pH=3 before mixing this POM with gelatin. The stability of $[BW_{12}O_{40}]^{5-}$ in those physical-chemical conditions has thus been studied by recording solution ^{11}B NMR spectra and cyclic voltammograms. The solution ^{11}B NMR spectra of $[BW_{12}O_{40}]^{5-}$ in aqueous solutions of pH=4.7 (solution obtained by dissolution of $K_5[BW_{12}O_{40}].11H_2O$ in water, see experimental part) and pH=3 are almost

identical (Fig. S1(a)-(b) of ESI). Both spectra display a sharp NMR signal close to 1.8 ppm ($\Delta\nu_{1/2}$= 5 Hz) which is characteristic of a boron nucleus in a tetrahedral environment. The cyclic voltamogramm (CV) of $[BW_{12}O_{40}]^{5-}$ at pH=3 is presented in Fig.2(a) with a scan rate of 10 mV.s^{-1}. The CV of $[BW_{12}O_{40}]^{5-}$ was also recorded at higher scan rate (100 mV. s^{-1}) in order to evidence clearly the redox peaks of $[BW_{12}O_{40}]^{5-}$ (see Fig. S1(c)). Redox peaks E_1-E_1', E_2-E_2', E_3 correspond to reduction and oxidation peaks of $[BW_{12}O_{40}]^{5-}$. In the potential range studied (+0.4 to -0.9 V), the dissolved $[BW_{12}O_{40}]^{5-}$ displays two reversible one-electron peaks (noted E_1 and E_2) situated at mean peak potentials ($E_{½}$=Ep_a + Ep_c)/2) of -0.45 V and -0.66 V vs Ag/AgCl, respectively. When scanning to more cathodic potential, a third four-electron non-reversible peak (E_3) is observed at -0.79 V vs Ag/AgCl. This CV is fully consistent with that reported previously for $[BW_{12}O_{40}]^{5-}$ at pH=3.[43] The electrochemical reactions associated to these peaks can be expressed as follows:

(E_1) $[BW_{12}O_{40}]^{5-} + e^- \rightarrow [BW_{12}O_{40}]^{6-}$ (1)

(E_2) $[BW_{12}O_{40}]^{6-} + e^- \rightarrow [BW_{12}O_{40}]^{7-}$ (2)

(E_3) $[BW_{12}O_{40}]^{7-} + 4e^- + xH^+ \rightarrow H_x[BW_{12}O_{40}]^{(11-x)-}$ (3)

While the first and second peaks are almost pH independent at 3<pH<7, it has been shown that the third irreversible peak is strongly pH dependent and its peak potential shifts to negative values with increasing pH.[43] This shift of redox potentials is quite common in polyoxometalates, where the uptake of protons during reduction of POM is to counterbalance the increase of charge density on the POM (accumulation of electrons). The CV of $[BW_{12}O_{40}]^{5-}$ at pH=3 is consistent with the solution ^{11}B NMR spectrum, showing that the structure of $[BW_{12}O_{40}]^{5-}$ is preserved at pH=3 and low concentration (0.5 mM).

3.2 Complex coacervation process between $[BW_{12}O_{40}]^{5-}$ and gelatin

The macroscopic behaviour of gelatin solutions in presence of $[BW_{12}O_{40}]^{5-}$ complexes

has been investigated in acidic conditions (pH = 3.0 ± 0.1) at T = 40 °C. By increasing the POM concentrations (0.3-10 mM) while keeping the gelatin concentration constant (3.33 wt%), three different states of $[BW_{12}O_{40}]^{5-}$-gelatin mixtures can be distinguished after 2 min of mixing both components (i) a white transparent solution (samples C and D of Fig. 3); (ii) white turbid solutions (sample E of Fig. 3); (iii) macroscopically biphasic samples composed of a dilute solution of $[BW_{12}O_{40}]^{5-}$ and gelatin floating above a dense white viscous phase (sample F of Fig. 3). Turbid solutions (sample E) are metastable and evolve kinetically upon ageing to macroscopic biphasic samples (similar to sample F). In contrast, samples C and D remain macroscopically stable upon ageing. These macroscopic observations have been confirmed by QELS (Fig.S2 of ESI) since colloids with Rh = 500 nm (i.e. 25 times the hydrodynamic radius of bare gelatin coil which is close to 20 nm[44]) have been evidenced 2 min after mixing gelatin and POM solutions in samples C and D while sample E is characterised by a slow aggregation process. Indeed, when monitoring the evolution upon ageing of a transparent solution prepared at very low gelatin and POM concentrations ([G] ~0.375 mM and $[BW_{12}]$~0.23 mM), an increase of the mean diameter of about 23 % in 4 h was observed (see Fig. S2 of ESI). Such a behaviour is comparable to that obtained with the $[H_2V_{10}O_{28}]^{4-}$/gelatin system[26] and consistent with a two-steps coacervation process (i.e. liquid-liquid phase separation in colloidal systems).[7,45] As mentionned above, similar liquid-liquid phase separation in systems involving bio-polyelectrolytes and oppositely charged colloids are generally described by a complex coacervation behaviour.[28,29,45] Scheme 1 represents a simple mechanism corresponding to the three states of the $[BW_{12}O_{40}]^{5-}$/gelatin system. For low $[BW_{12}O_{40}]^{5-}$ concentration, complexes between $[BW_{12}O_{40}]^{5-}$ and individual protonated gelatin chains are formed due to their attractive electrostatic interactions. Upon increasing $[BW_{12}O_{40}]^{5-}$ concentration, inter-polymer aggregates are formed due to the physical cross-linking with other gelatin

chains. Once a critical cross-link density is reached, the inter-polymer structure collapses into micro-gel aggregates (coacervate sol). In a final stage, the low electrostatic repulsions between weakly-charged aggregates allow the progressive growth of aggregates until the macroscopic phase separation (coacervate phase). For gelatin ([G]=3.33 wt%) and $[BW_{12}O_{40}]^{5-}$ ($[BW_{12}]$ = 10 mM) solutions, a white viscous coacervate (Fig. 1(a)) has been isolated from the supernatant solution, dried at room temperature and characterised by FT-IR and ^{11}B MAS NMR spectroscopies (Fig. 1(b)-(c)). The FT-IR spectrum displays characteristic vibration modes of the tungsten oxide skeleton of $[BW_{12}O_{40}]^{5-}$ and the carbon skeleton vibrations of gelatin (see Table 1 of ESI). The ^{11}B MAS NMR spectrum of $[BW_{12}O_{40}]^{5-}$-G hybrids (Fig. 1(b)) displays a single signal at 1.9 ppm, characteristic of a symmetric BO_4 environment, which is close to that observed within the potassium salt $K_5[BW_{12}O_{40}].11H_2O$ (single ^{11}B NMR resonance at 2.0 ppm). The characterisation of $[BW_{12}O_{40}]^{5-}$-G hybrids by FT-IR and solid state NMR spectroscopies are fully consistent with a strong immobilisation of the polyanion in the gelatin matrix and the retention of the Keggin molecular structure.

3.3 $[BW_{12}]$-G-ILGCE: optimisation of preparation, characterisation, voltammetry and stability.

For the preparation of electrodes based on $[BW_{12}O_{40}]^{5-}$/gelatin film, the glassy carbon electrode (GCE) has been first modified with imidazolium based ionic liquids (see experimental section). Actually, ionic liquids can be considered as “green” electrolytes exhibiting interesting electrochemical properties, namely a high conductivity and wide electrochemical window. They have already been employed to increase the electron transfer rate of different (bio)organic and inorganic electroactive species.[46] In particular, an increase in the sensitivity of the response toward the detection of nitrite has already been observed with carbon electrodes modified with imidazolium-based ionic liquid.[34,36]

In the present article, GCE have been modified with five ionic liquids [bmim] [X] (with X^- = PF_6^-, OTf^-, Cl^-, Br^-, BF_4^-) and a significant increase of the current baseline can be observed with ILGCE compared to GCE (see Fig. S3), as previously reported on carbon paste electrode (CPE) modified with [bmim] [PF_6][36]. The electrochemical response of these five ILGCE differing by the nature of X^- has been compared in 0.5 M Na_2SO_4 aqueous solution at pH=3. Since the highest increase of the current base line is obtained with [bmim] [PF_6] (Fig. 4), this ionic liquid has been selected for the preparation of modified electrode based on [BW_{12}]/gelatin film. This increase of the current baseline may be explained by a modification of the interface GCE/electrolyte by the ionic liquid. Actually, impedance and cyclic voltammetry experiments reported on [bmim][PF_6]/CPE have shown that ILs possibly act as a source of ion carriers to transport charges between carbon layers.[36] Therefore, according to this previous work, IL itself presents a good ionic conductivity and inherent capacitive quality. In the present work, it may be suggested that the conductive performance of ILGCE is notably higher than GCE due to a mixed electronic (carbon) and ionic (IL) contribution. Moreover, it is noteworthy that the modification of GCE with IL makes compatible the interface between hydrophilic species (gelatin and POMs) and a non polar surface (GCE).

The immobilisation of $[BW_{12}O_{40}]^{5-}$ at the surface of the ILGCE has been performed through a layer-by-layer deposition method of successively POM and gelatin charged species. Actually, the direct immobilisation of $[BW_{12}O_{40}]^{5-}$ on ILGCE is not efficient since no $[BW_{12}O_{40}]^{5-}$ can be electrochemically detected at the surface of the electrode (see CV of [BW_{12}]-ILGCE in Fig. S4(a) of ESI). As a consequence, the [BW_{12}]-G-ILGCE (1 POM layer) has been prepared by deposition of $[BW_{12}O_{40}]^{5-}$ on the ILGCE as a first layer and gelatin as a second layer. The POMs are then sandwiched between two charged surfaces (i.e. [bmim][PF_6] and gelatin) where the interface cohesion is ensured through

electrostatic interactions. The CV of $[BW_{12}]$-G-ILGCE shows three cathodic peaks characteristic of $[BW_{12}O_{40}]^{5-}$ (Fig. S4(b) of ESI) in the +0.4 to -1.0 V potential range. However, the low intensity of the peak currents suggests that a small amount of POMs is encapsulated in the IL/gelatin film. Therefore, deposition of an additional POM layer at the surface of $[BW_{12}]$-G-ILGCE has been performed, leading to 2$[BW_{12}]$-G -ILGCE (2 POM layers). This modified electrode is represented in scheme 3. The CV of the immobilised $[BW_{12}O_{40}]^{5-}$ exhibits the characteristic peaks E_1, E_2 and E_3 of $[BW_{12}O_{40}]^{5-}$ (Fig. 2(b))[32,43]. While the E_1 and E_2 peaks have mean potential values (-0.42 and -0.67 V vs Ag/AgCl respectively) similar to that of $[BW_{12}O_{40}]^{5-}$ in solution (see Fig. 2(a)), the peak E_3 at mean potential of -0.89 V is shifted to negative values which is consistent with the strong dependence of this peak with pH (*vide supra*). Moreover, compared to the dissolved $[BW_{12}O_{40}]^{5-}$ at pH = 3 (see Fig. 2(a)), the relative peak current of E_3 is notably lower. Since this redox reaction implies $4H^+$ per $[BW_{12}O_{40}]^{7-}$ (eq. 3), it may be suggested that the transfer of protons across the gelatin matrix may be partially hindered, thereby limiting this redox reaction. According to these observations, the local microenvironment of $[BW_{12}O_{40}]^{5-}$ in the IL/gelatin hydrogel is possibly at a pH value slightly higher than 3, in agreement with the pH buffering properties of gelatin. Compared to $[BW_{12}]$-G-ILGCE, the CV of 2$[BW_{12}]$-G-ILGCE presents higher peak currents, suggesting that a larger amount of POMs is retained and stabilized in the modified electrode with two POM layers. Moreover, the high porosity of the gelatin hydrogel as well as the attractive interactions between gelatin and $[BW_{12}O_{40}]^{5-}$ may enhance the diffusion of POMs in the gelatin matrix. The effect of the scan rate on the variation of the cyclic voltammograms has been investigated for 2$[BW_{12}]$-G-ILGCE (see Fig. 5). The cathodic peak potentials shift to more negative values and the corresponding anodic peak potentials to more positive values with increasing scan rate. The reversibility of the electrochemical process

decreases when the scan rate increases. The plots of peak current (I_1) versus scan rates are shown in the inset of Fig. 5. At scan rates higher than 50 mV.s^{-1}, the peak currents are proportional to the square root of the scan rate and the peak-to-peak potential separation (ΔE_p) increases with the scan rate. These results are consistent with a diffusion-controlled redox process. At these scan rates, the charge transfer kinetics is certainly limited by the electron hopping across the gelatin layer. However, at scan rates lower than 50 mV.s^{-1}, while all the peak potentials remain almost constant, the peak currents increase linearly with scan rate, suggesting a quasi-reversible surface-confined redox process. Such a relationship is consistent with a fast dynamics of charge transport at ionic liquid [bmim][PF_6]/GCE modified electrode. The influence of the gelatin concentration on the electrochemical properties of 2[BW_{12}]-G-ILGCE has been studied. By increasing the gelatin concentration up to 3 wt% (see Fig. S5(a) of ESI), a significant decrease of the anodic and cathodic currents is clearly observed which may be explained by a poor charge transfer. In contrast at gelatin concentration lower than 1 wt%, a significant leaching of POM species from the modified electrode is clearly observed in solution, as a consequence of a too low amount of gelatin molecules at the surface of the electrode for an efficient immobilisation of POMs. Moreover, at such low gelatin concentrations, the physical reticulation of gelatin macromolecules into hydrogel presumably does not occur, leading to a possible redissolution of gelatin after dipping the modified electrode in the aqueous electrolyte. Therefore, the gelatin concentration has been fixed at 1 wt% which seems to be a good compromise for the preparation of modified electrodes. The surface concentration in electroactive species can be calculated by integration of peak current recorded at low scan rate (ν < 50 mV/s) (Fig. 2(b)) based on the equation (4)[47]:

$$I_p = \frac{n^2F^2A\Gamma\upsilon}{4RT} = \frac{nFQ\upsilon}{4RT} \qquad (4)$$

Where I_p is the peak current, Γ is the surface coverage of the electroactive species (mol. cm^{-2}), A the electrode surface area (0.07 cm^2), Q the quantity of charge (C) which is calculated from the peak area of the cyclic voltammogram, ν the sweep rate and n the number of electrons transferred per electroactive species. Other symbols have usual meanings.

From Eq. (4), Γ can be calculated according to the following equation:

$$\Gamma = \frac{Q}{nFA} \quad (5)$$

The surface coverage, Γ, of $[BW_{12}O_{40}]^{5-}$ at 2[BW_{12}]-G-ILGCE is equal to $1.86.10^{-7}$ mol.cm^{-2}, which is close to the total amount of POM deposited at the surface of the electrode (i. e. ≅$1.42.10^{-7}$ mol.cm^{-2}).

Long term stability of the 2[BW_{12}]-G-ILGCE has been studied by comparing the change in voltammetric peak current of the modified electrode before and after potential cycling for 20 min in buffer solution of pH=3. 2[BW_{12}]-G-ILGCE has shown stable potentiodynamic responses as demonstrated by only minor differences between the 1st and 50th cyclic voltammograms (see Fig.S5(b)). Furthermore, no significant decrease has been revealed after replacing the 0.5 M Na_2SO_4 electrolyte used for 50 repetitive cycles with fresh solution. These results show that $[BW_{12}O_{40}]^{5-}$ is significantly anchored in this multilayer gelatin film. The storage stability of 2[BW_{12}]-G-ILGCE has also been estimated. A 2[BW_{12}]-G-ILGCE has been stored in its 0.5 M Na_2SO_4 aqueous solution at pH=3 and 4°C. No decrease of the peak currents is observed after one week. A slight decrease of the signal (ca. 6% after 5 days) is observed afterwards.

Characterisation of the surface morphology of the 2[BW_{12}]-G-IL film has been carried out by combining SEM-FEG and AFM microscopies. The SEM-FEG images of the 2[BW_{12}]-G-IL (Fig. 6) show that the hybrid film is a uniform and porous network which apparently results from the aggregation of particles. In contrast, the gelatin film presents a very smooth surface (see Fig.S6 of ESI) as already reported[48]. Spherical aggregates with a very large

distribution of diametres (typically between 100 nm and 10 μm) are also present on the surface of the 2[BW_{12}]-G-IL film. The characterisation of similar hybrid films prepared with a lower volume of solution deposited, confirms that the network is made of interconnected aggregates (Fig. S7 of ESI). The size distribution of these aggregates comprised between 300 and 800 nm is consistent with that measured by DLS on diluted gelatin- $[BW_{12}O_{40}]^{5-}$ solutions (*vide supra*), suggesting that the complexation process taking place at the electrode interface is comparable to the complex coacervation process previously identified in bulk. The distribution of gelatin and $[BW_{12}O_{40}]^{5-}$ in the 2[BW_{12}]-G-IL coating is studied by recording SEM images with elemental mapping via EDX analysis. The elemental mapping on the rectangular area shown in Fig. 7 and Fig. S8 of ESI demonstrates an excellent uniform distribution of C, N, O and W elements. Atomic percentages from EDX elemental analysis were found to be 67±4, 15±1, 17±3 and 1.0±0.4 for C, N, O and W respectively. It is noteworthy that the aggregates present at the surface of the film are characterised by a small amount of gelatin (low atomic percentage for C, N and O elements), suggesting the assembly of $[BW_{12}O_{40}]^{5-}$ clusters interconnected with a few gelatin chains. Topographical characterisation was conducted by tapping mode atomic force microscopy (AFM). The images (1 μm x 1 μm) were recorded at low scan rate (0.5Hz). The [BW_{12}]-G-IL film (Fig. 8) exhibits a rough granular surface composed of homogeneously distributed rod-like aggregates whose size ranges approximately from 20 to 100 nm.

3.4 Electrocatalytic reduction of nitrite at 2[BW_{12}]-G-ILGCE

As POMs can serve as powerful electron reservoir, they are well known as electroactive species widely used for electrocatalytic reductions. In particular, Dong *et al* have shown that $[SiW_{12}O_{40}]^{4-}$ can be used as an electrocatalyst for the the reduction of nitrite.[49] Keita *et al* demonstrated that Keggin-type and Dawson-type POMs incorporated in conducting polymers

present electrocatalytic properties towards the reduction of nitrite.[19a] Up to now, a series of POMs of different functionality has been recognized and proved interesting catalysts for the electroreduction of nitrite by reducing the overpotential.[22,34,36] However, for most of the modified POMs electrodes reported so far, the titration of nitrite is generally performed at pH≤1 (H_2SO_4 electrolyte) due to the hydrolysis of POMs at higher pH.[16a,24,25,34,37] In the present work, we show that nitrite can be detected in milder conditions (pH 3) due to the stabilization of $[BW_{12}O_{40}]^{5-}$in the gelatin/IL film. Fig. 9 shows the voltammetric behaviour of 2[BW_{12}]-G-ILGCE towards the electrocatalytic reduction of nitrite at pH=3. In the potential range studied, no direct reduction of nitrite could be observed at gelatin/ILGCE while upon nitrites addition, the 2[BW_{12}]-G-ILGCE exhibits a significant increase of the cathodic currents and a concomitant decrease of the anodic currents. Such results indicate the electrocatalytic reduction of nitrites by $[BW_{12}O_{40}]^{5-}$. The catalytic current appears on the three cathodic peaks despite being stronger for the second and third ones. The characteristics of the present nitrite sensor along with other reported POM based sensors are listed in Table 1. The inset of Fig. 9 shows a linear relationship between the catalytic current taken at -0.72 V vs Ag/AgCl and the concentration of nitrite. A current response of ~61.6 $mA.M^{-1}$ (868 $mA.M^{-1}.cm^{-2}$) nitrite is observed over a dynamic concentration range between 50 and 600 μM. This is one of the highest sensitivity reported so far for POM based nitrite sensors (see Table 1). The limit of detection (LoD = 16 μM) is estimated from the linear calibration plot (X_{LoD} = (a+ 3Sa)/b).[50] The stability and reproducibility of the present sensor was evaluated for 5 repetitive measurements in the buffer solution containing 100 μM of nitrite. The repeatability of the titration has also been evaluated for four other nitrite concentrations (200, 300, 400 and 500 μM). For the five concentrations, it has been found that the standard deviation of the response current to nitrite does not exceed 1%. These results demonstrate that 2[BW_{12}]-G-ILGCE based sensor is considerably stable and repeatable.

4. Conclusions

There is currently a strong demand for producing multifunctional materials with minimal environmental impact. These materials have to be synthesised in chemical conditions (temperature, pH, concentrations…) compatible with the preservation of the chemical structure and physical-chemical properties of the different components. Moreover, the performance of nanocomposites in applications requires the control over the morphology, surface structure and interfacial properties between inorganic and (bio)organic components.[51]

In this work, bionanocomposite films have been processed by interfacing a polyoxotungstate cluster (i. e. $[BW_{12}O_{40}]^{5-}$) and a biopolymer (i. e. gelatin) on a glassy carbon electrode. The assembly of both components is carried out in peculiar physical-chemical conditions that optimise the charge matching between both components (i. e. the anionic POMs and the cationic gelatin). Actually, the charge density of gelatin macromolecules can be tuned by adjusting pH and for pH <4, strong electrostatic interactions between $[BW_{12}O_{40}]^{5-}$ and gelatin macromolecules give rise to a complex coacervation phenomenon that leads to a hybrid hydrogel.

Looking for the building-up of a sensing device based on electroactive polyoxometalate, we have shown that the coacervation process can be an efficient approach to strongly immobilise $[BW_{12}O_{40}]^{5-}$ clusters at the surface of a glassy carbon electrode (GCE). The preparation of the modified electrode based on a layer-by-layer approach is an easy, readily controlled method using gelatin as a renewable host matrix because of its high abundance, low cost and absence of toxicity. Thus, the modified electrode 2[BW_{12}]-G-ILGCE has been built up by the alternate deposition of oppositely charged species (POMs and gelatin) on GCE modified by imidazolium based ionic liquid (ILGCE). The presence of the ionic liquid improves the interfacial properties between the $[BW_{12}O_{40}]^{5-}$/gelatin hydrogel and GCE as well as provides a remarkable increase of the charge transfer rate. This modified electrode presents

an excellent, very stable and reproducible electrochemical response, showing that the combination of ionic liquids and gelatin provides a suitable and stabilizing microenvironment for electroactive molecules such as POMs. Moreover, 2[BW_{12}]-G-ILGCE exhibits a good catalytic activity towards the reduction of nitrite since a high sensitivity (868 $mA.M^{-1}.cm^{-2}$), and a large linear range of nitrite concentrations (50-600 μM) have been measured. Further developments are now necessary to increase the electron transfer rate by controlling and optimising the thickness of the ionic liquid or gelatin layers and the number of POM/gelatin layers. More importantly, the substitution of synthetic polymers by natural macromolecules for the building-up of sensors may be enlarged to a wide panel of modified electrodes since this approach is advantageous, not only in terms of economic (high abundance, low cost) and environmental (non fossil source) impact, but also due to the wide range of available biopolymers exhibiting a tremendous diversity of chemical and structural properties. Such chemical multifunctionality is a key advantage for the entrapment of a large diversity of functional species including POM, molecular complexes[52] or biological catalysts such as enzymes or cells.[53]

Table 1. Electroanalytical properties of 2[BW_{12}]-G-ILGCE along with the other nitrite POM-based sensors.

Electrodes	pH	Applied potential (V) vs. Ag/AgCl	S[a] ($mA.M^{-1}$)/ S^{xa} ($mA.M^{-1}.cm^{-2}$)	LCR[b] (μM)	reference
[PMo_{12}]/IL[c]/GCE	1	-0.2	0.3939	330-3300	34
[PMo_{12}]/PAH[d]/IL[c]/GCE	1	-0.2	0.3463	330-3300	34
Tri[e]/PAH[d]/[PW_{18}]/Tri[e]/ PAH[d]/PSS[f]/ATS[g]/GCE[h]	1	-0.3	3.85	20-220	16a
[PW_{12}]/PV4P[i]/CNTs[j]/GCE	1	-0.65	-	1.2-17.5	21e
[P_2W_{18}]/PVA[k]/ITO[l]	1	-0.2	10.95	100-1500	25
[PMo_{12}]/IL[m]/CPE[n]	1	-0.001	1.8	1250-10^4	37
[SiW_{12}]/NB[o]/CPE[n]	1	-0.25	*178.2*	5-1200	24c
2[BW_{12}]-G-ILGCE	3	-0.72	61.6/*868.2*	50-600	tw[p]

[a] sensitivity; [b]linear concentration range; [c] Ionic Liquid: [bmim][BF_4]; [d] poly-allylamine-hydrochloride; [e] Triton X-405; [f] poly(sodium4-styrenesulfonate); [g] 3-aminotrimethoxysilane; [h] multilayer film with 10 POM layers; [i] poly(4-vinylpyridine) [j] carbon nanotubes, [k] poly(vinyl alcohol), [l] indium tin oxide,[m] Ionic Liquid: [emim] [n] carbon paste electrode, [o] Nile blue,[p] this work,

Caption of scheme

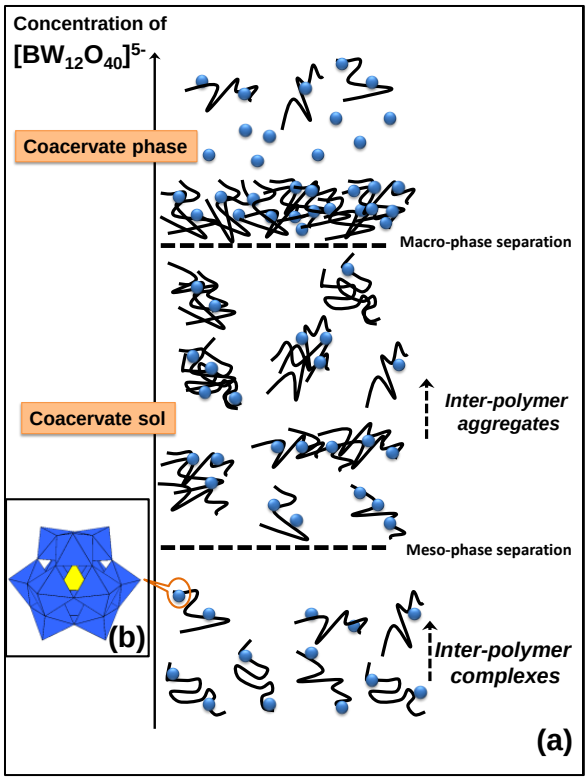

Scheme 1 Proposed schematic representation of the complex coacervation mechanism between $[BW_{12}O_{40}]^{5-}$ (blue disk) and gelatin chains (black lines). (b) Polyhedral representation of the polyanion $[BW_{12}O_{40}]^{5-}$. WO_6 and BO_4 units are represented by blue octahedra and a yellow tetrahedron respectively.

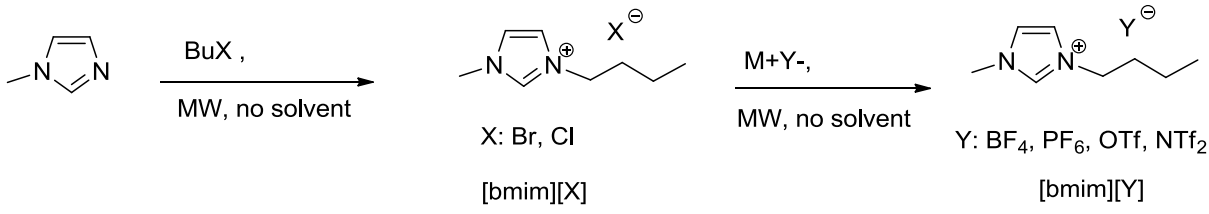

Scheme 2. Synthesis and characterisation of ionic liquids.[40]

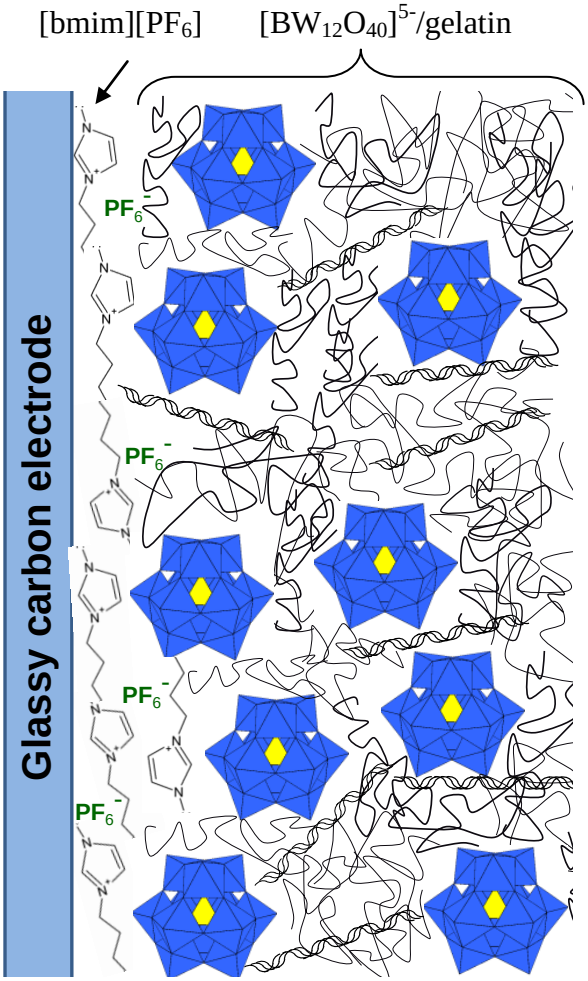

Scheme 3. Schematic representation of the 2[BW_{12}]-G-IL-GCE modified electrode.

Caption of figures

Figure 1. (a) Photograph of a $[BW_{12}]$-G coacervate prepared with 5 mL of a gelatin solution ([G]=10 wt%) and 10 mL of a $[BW_{12}O_{40}]^{5-}$ solution ($[BW_{12}]$ =15 mM) (b) ^{11}B MAS NMR spectra and (c) FT-IR spectra of $[BW_{12}]$-G coacervate (*red line*) and potassium salt $K_5[BW_{12}O_{40}].11H_2O$ (*blue line*).

Figure 2. Cyclic voltammograms of (a) dissolved $[BW_{12}O_{40}]^{5-}$ (c = 5.10^{-4} $mol.L^{-1}$) in $CHCl_2COOH/CHCl_2COONa$ 1M-1M at pH 3, (b) immobilised $[BW_{12}O_{40}]^{5-}$ in 2$[BW_{12}]$-G-ILGCE. Electrolyte 0.5 M Na_2SO_4 aqueous solution at pH 3. Scan rate: 10 mV s^{-1}.

Figure 3. Photographs of samples taken few minutes after preparation. Samples (A) and (B) correspond respectively to pure gelatin ([G] =3.33 wt.% (~ 0.83 mM)) and $[BW_{12}O_{40}]^{5-}$ solutions ($[BW_{12}]$ = 0.3 mM) while others samples were prepared at constant gelatin concentration ([G] = 0.83 mM) and increased $[BW_{12}O_{40}]^{5-}$ concentrations (0.2 mM for sample C, 0.3 mM for sample D, 0.66 mM for sample E, 1.32 mM for sample F).

Figure 4. Residual currents recorded at GCE modified with different ionic liquids (i.e.[bmim][X], with X^-=PF_6^-,BF_4^-, Cl^-, Br^- and OTf^-) in 0.5 M Na_2SO_4 aqueous solution at pH 3. Scan rate: 10 mV s^{-1}.

Figure 5. Cyclic voltammograms of 2$[BW_{12}]$-G-ILGCE in 0.5 M Na_2SO_4 aqueous solution at pH 3 at different scan rates (a) 10, (b) 50, (c) 100, (d) 150, (e) 200, (f) 250 $mV.s^{-1}$. The inset shows the dependence of the cathodic peak current at -0.48 V vs Ag/AgCl $[I_1p_c]$ on scan rates (*black circles*) and the square roots of scan rates (*white squares*).

Figure 6. (a) and (b) SEM images of 2[BW_{12}]-G-IL coatings prepared from the deposition of 2 x 20 μL of a 0.5 mM $[BW_{12}O_{40}]^{5-}$ solution and 20 μL of 1 wt% solution of gelatin.

Figure 7. (a) SEM image of a 2[BW_{12}]-G-IL coatings prepared from the deposition of 2 x 20 μL of a 0.5 mM $[BW_{12}O_{40}]^{5-}$ solution and 20 μL of 1 wt% solution of gelatin. (b-e) elemental mapping of carbon (b), nitrogen (c), oxygen (d) and tungsten (e) by EDX spectroscopy for the rectangular area indicated by the white box in panel (a).

Figure 8. AFM images of 2[BW_{12}]-G-IL coatings prepared from the deposition of 2 x 20 μL of a 0.5 mM $[BW_{12}O_{40}]^{5-}$ solution and 20 μL of 1 wt% solution of gelatin. (a) - (c) and (b)-(d) are height and amplitude profiles, respectively.

Figure 9. a) Cyclic voltammograms of 2[BW_{12}]-G-ILGCE in 0.5 M Na_2SO_4 aqueous solution at pH 3 containing (a) 0.0; (b) 100; (c) 200; (d) 300; (e) 400; (f) 500; (g) 600 μM nitrite. Inset shows calibration curve of current vs nitrite concentration at potential applied of -0.72 V vs Ag/AgCl. Scan rate: 10 $mV.s^{-1}$.

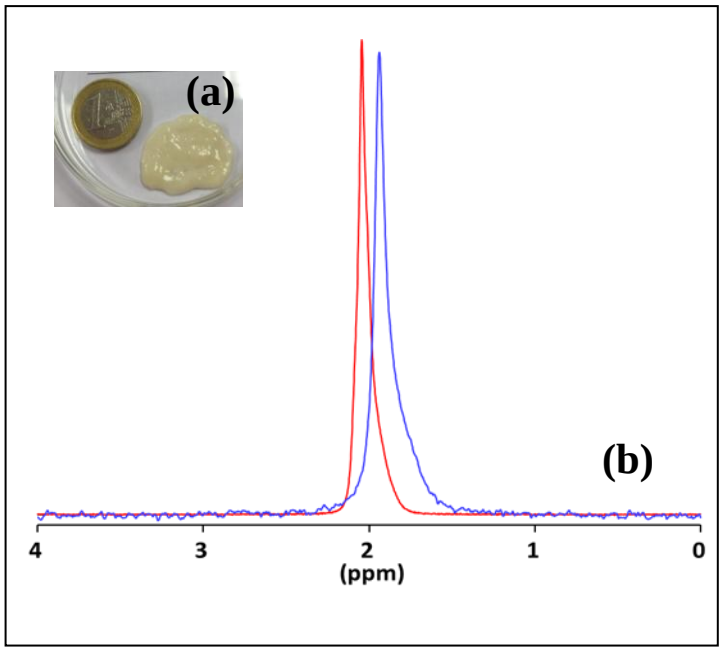

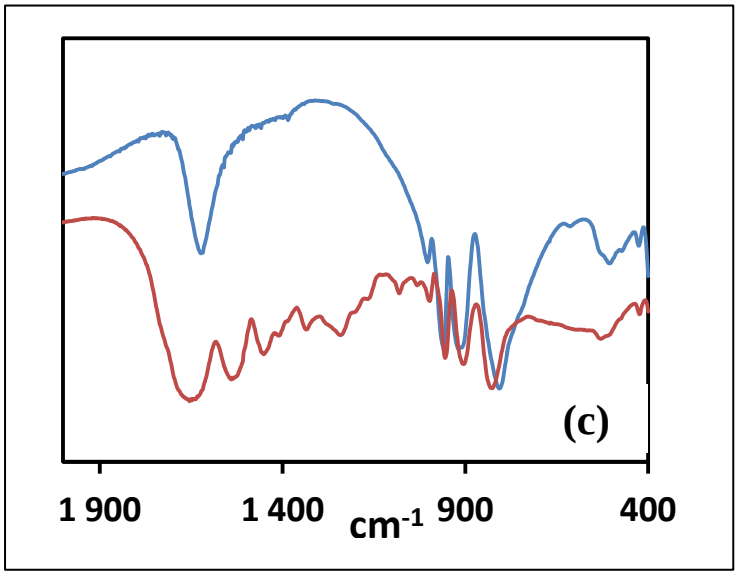

Figure 1

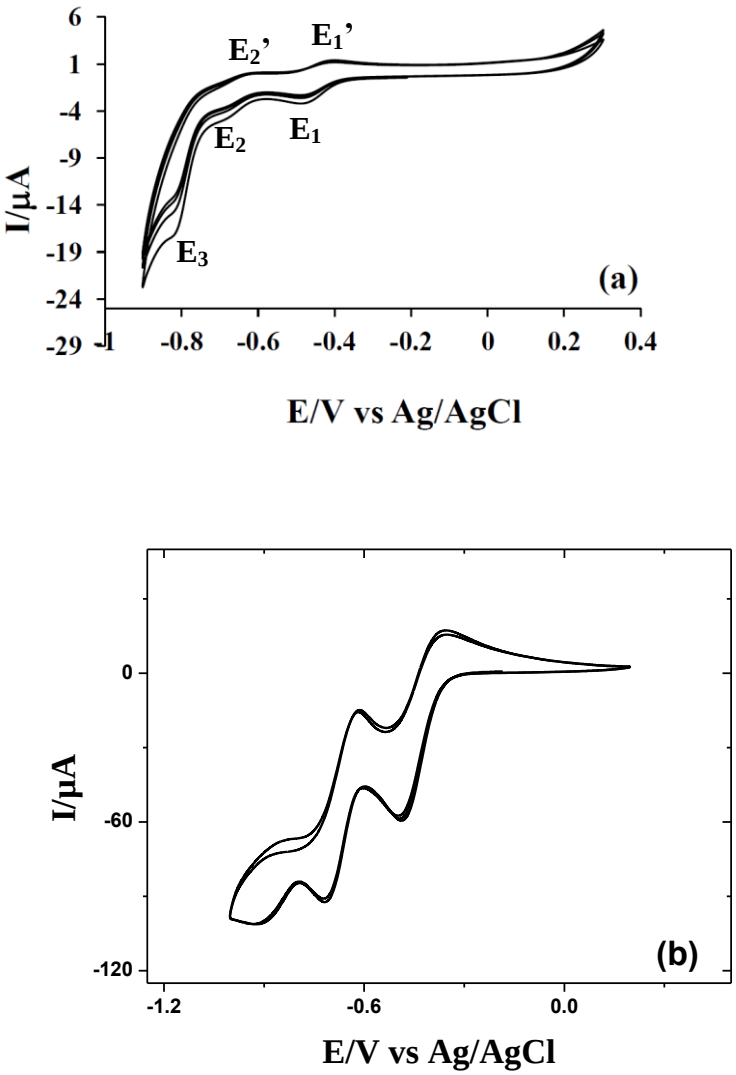

Figure 2

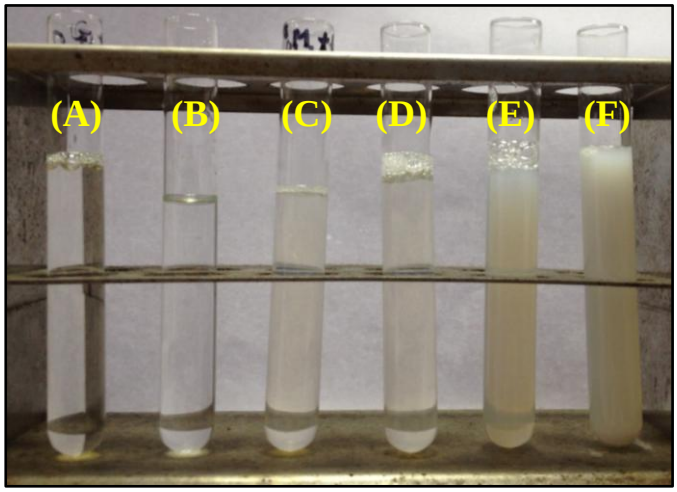

Figure 3

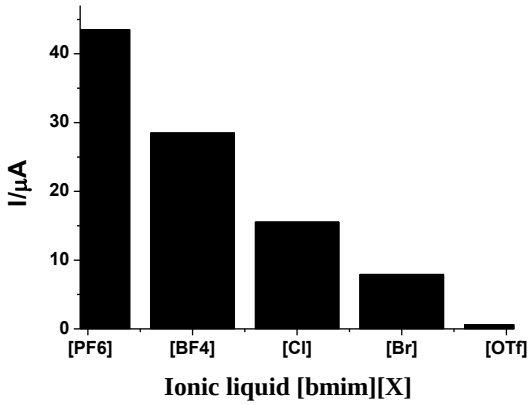

Figure 4

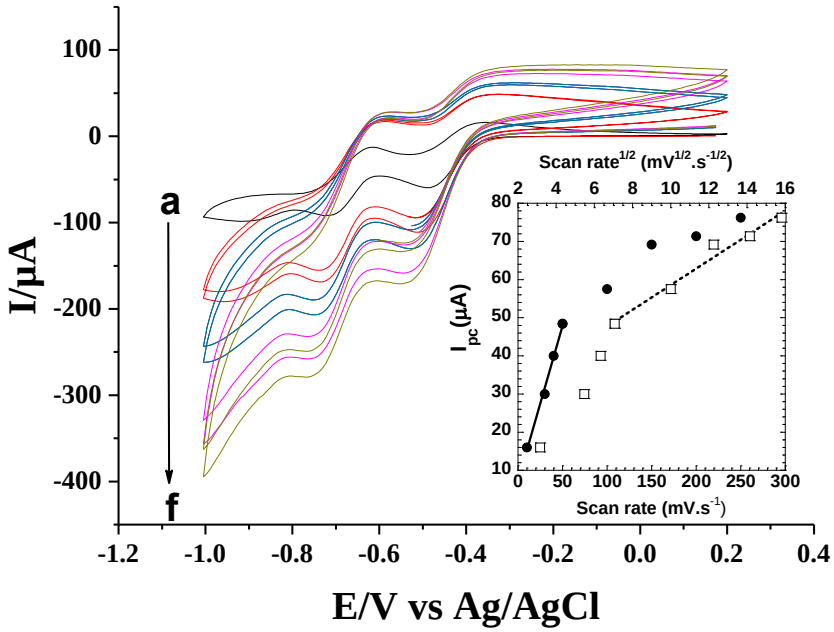

Figure 5.

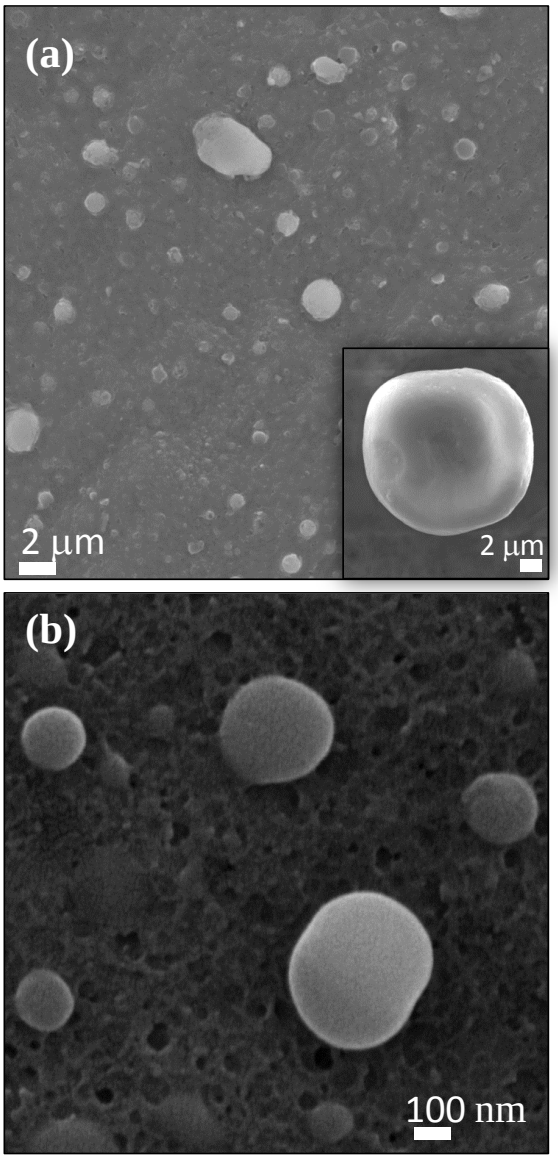

Figure 6.

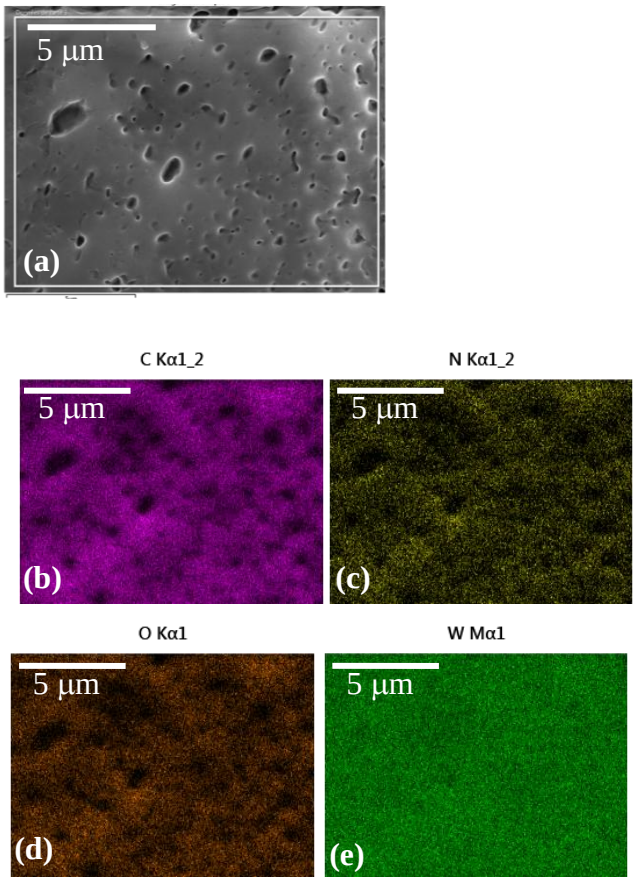

Figure 7

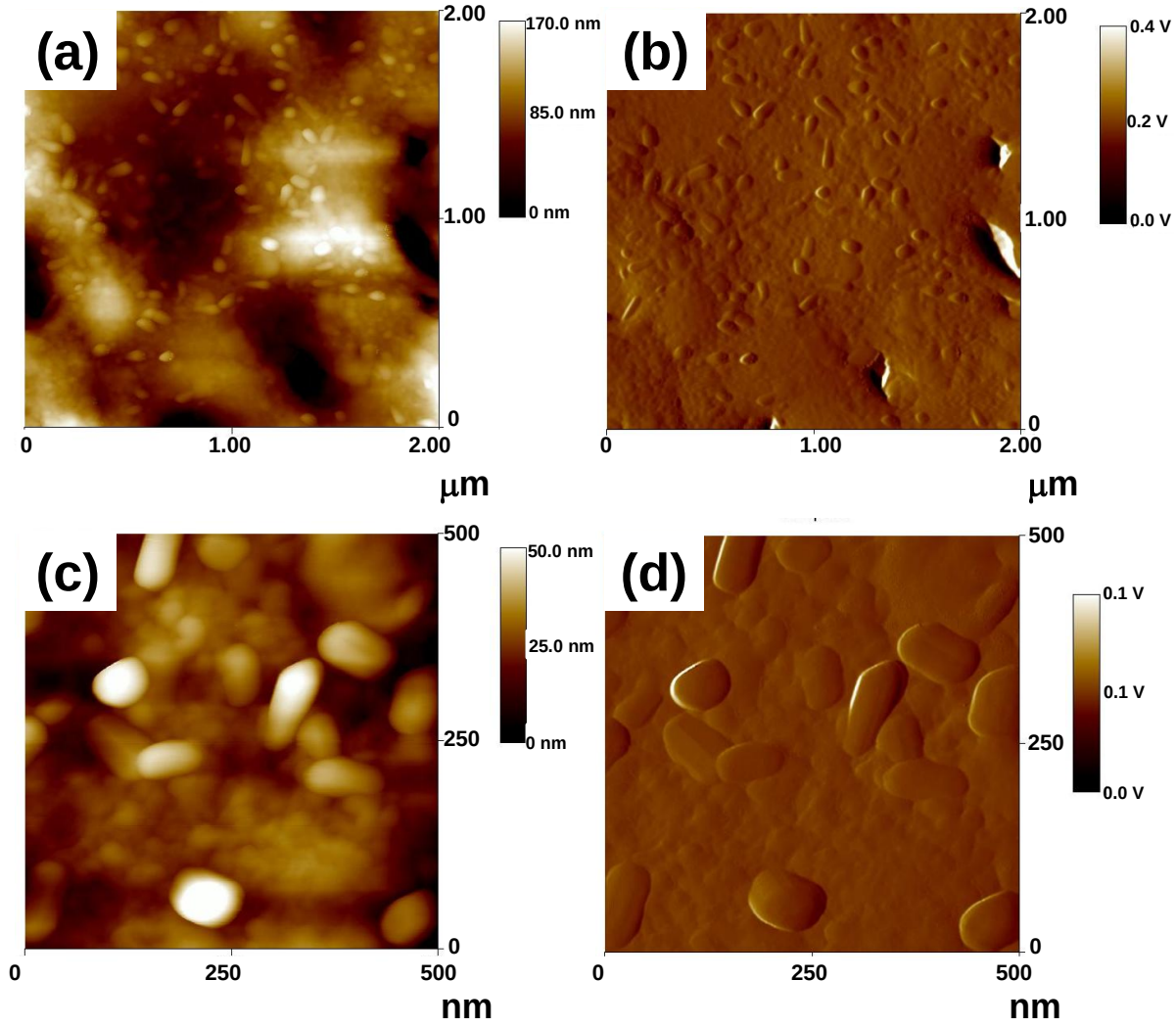

Figure 8

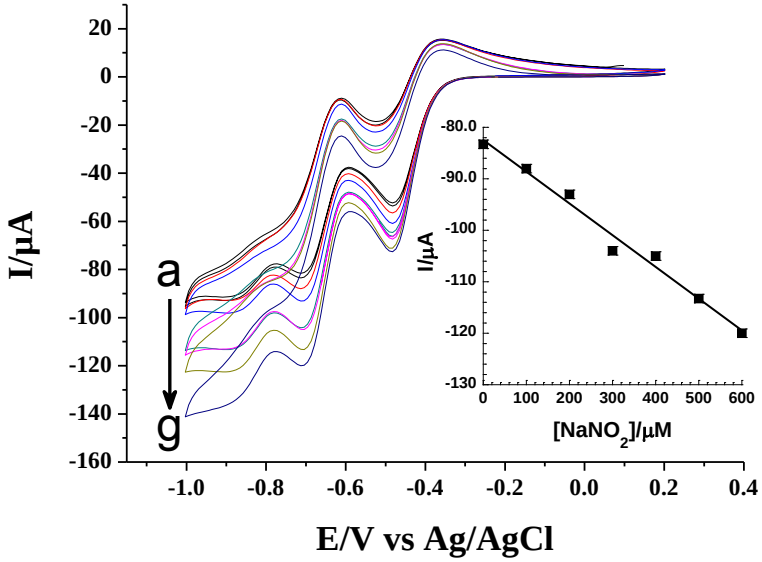

Figure 9

5. REFERENCES

1 (a)Y. Aouat, G. Marom, D. Avnir, V. Gelman, G. E. Shter, G. S. Grader, *J. Phys. Chem. C,* 2013, **117**, 22325; (b) L. Shapiro, D. Avnir, *ChemCatChem,* 2013, **5**, 2195; (c) O. L. Muskens, M. W. England, L. Danos, M. Li, S. Mann, *Adv. Funct. Mater.*, 2013, **23**, 281; (d) L. Turyanska, T. D. Bradshaw, M. Li, P. Bardelang, W. C. Drewe, M. W. Fay, S. Mann, A. Patane, N. R. Thomas, *J. Mater. Chem.*, 2012, **22**, 660.

2 (a) C. X. Guo, S. Huang , X. Lu *Green Chem.*, 2014, ASAP, DOI: 10.1039/ C3GC42645A; (b) L. Johnson, W. Thielemans, D. A. Walsh, *Green Chem.*, 2011, **13**, 1686.

3 M. Darder, P. Aranda, E. Ruiz-Hitzky, *Adv. Mater.*, 2007, **19**, 1309; (b) M. Darder, P. Aranda, M. L. Ferrer, M. C. Gutierrez, F. del Monte, E. Ruiz-Hitzky, *Adv. Mater.*, 2011, **23**, 5262 ; (c) S. Mann, *Nature Mater*., 2009, **8**, 781.

4 (a) C. Joly-Duhamel, D. Hellio, A. Ajdari, M. Djabourov, *Langmuir,* 2002, **18**, 7158; (b) C. Joly-Duhamel, D. Hellio, M. Djabourov, *Langmuir,* 2002, **18**, 7208.

5 (a) A. G. Ward, A. Courts, in *The Science and Technology of Gelatin*, Academic Press, London, 1977; (b) M. Djabourov, *Contemp. Phys.* 1988, **29**, 273; (c) S. B. Ross-Murphy, *Polymer,* 1992, **33**, 2622; (d) C. Michon, G. Cuvelier, B. Launay, *Rheol. Acta,* 1993, **32**, 94.

6 (a) T. Coradin, A. Marchal, N. Abdoul-Aribi, J. Livage, *Colloids Surf. B. Biointerfaces* 2005, **44**, 191; (b) J. Allouche, M. Boissière, C. Hélary, J. Livage, T. Coradin, *J. Mater. Chem*. 2006, **16**, 3120; (c) R. Sasai, H. Itoh, I. Shindachi, T. Shichi, K. Takagi, *Chem. Mater.* 2001, **13**, 2012; (d) A. Bigi, B. Bracci, S. Panzavolta, *Biomaterials,* 2004, **25**, 2893; (e) K. Furuichi, Y. Oaki, H. Imai, *Chem. Mater.,* 2006, **18**, 229; (f) Z. Yang, Y. Jiang, L. X. Yu, B. Wen, F. Li, S. Sun, T. Hou, *J. Mater. Chem.,* 2005, **15**, 1807.

7 (a) F. Carn, O. Durupthy, B. Fayolle, T. Coradin, G. Mosser, M. Schmutz, J. Maquet, J. Livage, N. Steunou, *Chem. Mater.*, 2010, **22**, 398.

8 (a) *Chem. Soc. Rev*., 2012, **41**, 7325 ; (b) A. Dolbecq, E. Dumas, C. R. Mayer, P. Mialane, *Chem. Rev.*, 2010**, 110**, 6009; (c) U. Kortz, A. Müller, J. Van Slageren, J. Schnack, N. S. Dalal, M. Dressel, *Coord. Chem. Rev.*, 2009, **253**, 2315; (d) M. N. Sokolov, S. A. Adonin, P. A. Abramov, D. A. Mainichev, N. F. Zakharchuk, V. P. Fedin, *Chem. Commun.*, 2012, **48**, 6666 ; (e) M. N. Sokolov, S. A. Adonin, D. A. Mainichev, P. L. Sinkevich, C. Vicent, N. B. Kompankov, A. L. Gushchin, V. A. Nadolinny, V. P. Fedin, *Inorg. Chem.*, 2013, **52**, 9675.

9 (a) S. M. Ashraf, S. Kaleem, *Anal. Biochem.*, 1995, **230**, 68; (b) V. Ball, M. Barsukova-Stuckart, U. Kortz, *Colloid Polym. Sci.*, 2013, **291**, 1219 ; (c) G. Raj, C. Swalus, A. Guillet, M. Devillers, B. Nysten, E. M. Gaigneaux, *Langmuir*, 2013, **29**, 4388 ; (d) F. Carn, F. Boue, M. Djabourov, N. Steunou, T. Coradin, J. Livage, S. Floquet, E. Cadot, E. Buhler, *Soft Matter*, 2012, **8**, 2930 ;(e) H. Li, W. Qi, W. Li, H. Sun,W. Bu, L.Wu, *Adv. Mater.*, 2005, **17**, 2688; (f) V. Ball, C. Ringwald, J. Bour, M. Michel, R. Al-Oweini, U. Kortz, *J. Colloid. Inter. Sci.*, 2013, **409**, 166.

10 (a) D-L Long, R. Tsunashima, L. Cronin, *Angew. Chem. Int. Ed.*, 2010, **49**, 1736 ; (b) C. P. Pradeep, M. F. Misdrahi, F.Y. Li, J. Zhang, L. Xu, D. L. Long, T. Liu, L. Cronin, *Angew. Chem. Int. Ed.*, 2009, **48**, 8309.

11 (a) (d) Q. Zhang, L. He, H. Wang, C. Zhang, W. Liu, W. Bu, *Chem. Commun.*, 2012, **48**, 7067; (b) W. Bu, S. Uchida, N. Mizuno, *Angew. Chem. Int. Ed.*, 2009, **48**, 8281. (c) L. de Viguerie, A. Mouret, H-P. Brau, V. Nardello-Rataj, A. Proust, P. Bauduin, *CrystEngComm.*, 2012, **14**, 8446.

12 (a) R. Guo, Y.Cheng, D. Ding, X. Li, L. Zhang, X. Jiang, B. Liu, *Macromol. Biosci.*, 2011, **11**, 839; (b) J. Iqbal, M. Barsukova-Stuckart, M. Ibrahim, S. U. Ali, A. A. Khan, U. Kortz, *Medicin. Chem. Res.*, 2013, **22**, 1224.

13 (a) N. V. Maksimchuk, O. A. Kholdeeva, K. A. Kovalenko, V. P. Fedin, *Isr. J. Chem*,

2011, **51**, 281 ; (b) Y. Yan, L. Wu, *Isr. J. Chem*., 2011, **51**, 181; (c) M. Hutin, D. L. Long, L. Cronin, *Isr. J. Chem*., 2011, **51**, 205; (d) S. Berardi, M. Carraro, A. Sartorel, G. Modugno, M. Bonchio, *Isr. J. Chem*., 2011, **51**, 259.

14 (a)W. Sun, S. Zhang, X. Lin , L. Jin, S. Jin, J. Deng , J. Kong, *J. Electroanal. Chem*., 1999, **469**, 63; (b) A. Kuhn, F. C. Anson, *Langmuir*, 1996, **12**, 5481; (c) C. Rong, F. C. Anson, *Inorg. Chim. Acta*, 1996, **242**, 11.

15 (a) S. Zhai, J. Liu, J. Jiang, S. Dong, *Electroanalysis*, 2003, **15**, 1165; (b) L. Qian, X. Yang, *Electrochem. Commun.*, 2005, **7**, 547 ; (c) M. Ammam, B. Keita, L. Nadjo, J. Fransaer, *Sens. Actu. B.*, 2009, **142**, 347; (d) D. Fan, J.Hao, *J. Phys. Chem. B*, 2009, **113**, 21, 7513.

16 (a) M. Ammam, B. Keita, L. Nadjo, J. Fransaer, *Talanta*, 2010, **80**, 2132; (b) W. Zhu, W. Zhang, S. Li, H. Ma, W. Chen, H. Pang, *Sens. Actu. B.*, 2013, **181**, 773; (c) L. Kang, H. Ma, Y. Yu, H. Pang, Y. Song, D. Zhang, *Sens. Actu. B.*, 2013, **177**, 270 ; (d) A. F. Murphy, T. McCormac, *Electrochim. Acta*, 2011, **56**, 10751.

17 (a) A. Papadakis, A. Souliotis, E. Papaconstantinou, *J. Electroanal. Chem.*, 1997, **435**, 17; (b) D. F. Rohlfing, J. Rathousk, Y. Rohlfing, O. Bartels, M. Wark, *Langmuir*, 2005, **21**, 11320. (c) L. Li, W. Li, C. Sun, L. Li, *Electroanalysis*, 2002, **14**, 368.

18 (a) Y. Li, W. Bu, L. Wu, C. Sun, *Sens. Actu. B.*, 2005, **107**, 921. (b) H. Hamidi, E. Shams, B. Yadollahi, F. K. Esfahani, *Electrochim. Acta*, 2009, **54**, 3495 ; (c) A. L. Souza, L. A. Marques, M. N. Eberlin, P. A. P. Nascente, P. S. P. Herrmann Junior, F. L . Leite, U. P. Rodrigues-Filho, *Thin Solid films*, 2012, **520**, 3574.

19 (a) B. Keita, A. Belhouari, L. Nadjo, R. Contant, *J. Electroanal. Chem.*, 1995, **381**, 243; (b) A. Papadakis, A. Souliotis, E. Papaconstantinou, *J. Electroanal. Chem.*, 1997, **435**,17; (c) A. Mahmoud, B. Keita, L. Nadjo, O. Oung, R. Contant, S. Brown, Y de Kouchkovsky, *J. Electroanal. Chem.*, 1999, **463**, 129 ; (d) L. Adamczyk, P. J. Kulesza, K. Miecznikowski, B. Palys, M. Chojak, D. Krawczyk, *J. Electrochem. Soc.*, 2005, **152**, 3, E98; (e) W. Tao, Z. Li,

D. Pan, L. Nie, S. Yao, *J. Phys. Chem. B,* 2005**, 109**, 2666 (f) K. Foster, L. Bi, T. McCormac, *Electrochim. Acta*, 2008, **54**, 868.

20 W. Guo, L. Xu , F. Li, B. Xu, Y. Yang, S. Liu, Z. Sun, *Electrochim. Acta,* 2010, **55**, 1523.

21 (a) Z. Li, Ji. Chen, D. Pan, W. Tao, L. Nie, S. Yao, *Electrochim. Acta*, 2006, **51**, 4255; (b) A. Salimi, A. Korani, R. Hallaj, R. Khoshnavazi, H. Hadadzadeh, *Anal. Chim. Acta*, 2009, **635**, 63; (c) M. Skunik, P. J. Kulesza, *Anal. Chim. Acta*, 2009, **631**, 153; (d) W. Guo, L. Xu, B. Xu, Y. Yang, Z. Sun, S. Liu, *J. Appl. Electrochem.*, 2009, **39**, 647; (e) J. Yuan, X. Jin, N. Li, J. Chen, J. Miao, Q. Zhang, L. Niu, J. Song, *Electrochim. Acta*, 2011, **56**, 10069.

22 D. Zhang, H. Ma, Y. Chen, H. Pang, Y. Yu, *Anal. Chim. Acta*, 2013, **792**, 35.

23 T. Gan, C. Hu, Z. Chen, S. Hu, *Sens. Actu. B.*, 2010, **151**, 8.

24 (a) G. Xue, J. Xiong, H. Guo, G. Cao, S. Nie, H. Hu, *Electrochim. Acta*, 2012, **69**, 315; (b) G. Cao, J. Xiong, Q. Xue, S. Min, H. Hu, G. Xue, *Electrochim. Acta*, 2013, **106**, 465 ; (c) S. Kakhki, E. Shams, M. M. Barsan, *J. Electroanal. Chem.*, 2013, **704**, 80; (d) H-Y Zhang, A-J Miao, M. Jiang, *Mater. Chem. Phys.*, 2013, **141**, 482.

25 F. Cao, S. Guo, H. Ma, J. Gong, *Electroanal.*, 2012, **24**, 418.

26 F. Carn, N. Steunou, M. Djabourov, T. Coradin, F. Ribot, J. Livage, *Soft Matter*, 2008, **4**, 735.

27 F. Carn, M. Djabourov, T. Coradin, J. Livage, N. Steunou, *J. Phys. Chem. B*, 2008, **112**, 12596.

28 A. Veis and C. Aranyi, *J. Phys. Chem.*, 1960, **64**, 1203.

29 (*a*)Y.-F. Wang, J. Y. Gao, P. L. Dubin, *Biotechnol. Prog.*, 1996, **12**, 356; (b) S.L. Turgeon, C. Schmitt, C. Sanchez, *Curr. Opin. Coll. Interface Sci.*, 2007, **12**, 166; (c) A. F. Thunemann, M. Muller, H. Dautzenberg, J.F. Joanny, H. Lowen, *Adv. Polym. Sci.*, 2004, **166**, 113; (d) E. Kizilay, A. B. Kayitmazer, P. L. Dubin, *Adv.Coll. Interface Sci.*, 2011, **167**, 24.

30 (*a*) L. A. Luzzi, R. J. Gerraughty, *J. Pharm. Sci.*, 1967, **56**, 634; (b) P. L. Madan, D. K.

Madan, J. C. Price, *J. Pharm. Sci.*, 1976, **65**, 1476; (c) C. L. Cooper, P. L. Dubin, A. B. Kayitmazer, S. Turksen, *Curr. Opin. Colloid. Interface. Sci.* 2005, **10**, 52.

31 Y.-F. Wang, J. Y. Gao, P. L. Dubin, *Biotechnol. Prog.* 1996, **12**, 356.

32 L. Adamczyk, K. Miecznikowski, *J. Solid State Electrochem.*, 2013, **17**,1167.

33 H. Ji, L. Zhu, D. Liang, Y. Liu, L. Cai, S. Zhang, S. Liu, *Electrochim. Acta*, 2009, **54** 7429.

34 B.-Q. Huang , L. Wang, K. Shi, Z.-X. Xie, L.-S. Zheng, *J. Electroanal. Chem.*, 2008, **615**, 19.

35 B. Haghighi, H. Hamidi, L. Gorton, *Electrochim. Acta*, 2010, **55**, 4750.

36 H. Liu, P. He, Z. Li, C. Sun, L. Shi, Y. Liu, G. Zhu, J.Li, *Electrochem. Comm.*, 2005, **7**, 1357.

37 R. Wang, D. Jia, Y. Cao, *Electrochim. Acta*, 2012, **72**, 101.

38 (a) H. Chen, C. Mousty, S. Cosnier, C. Silveira, J. J. G. Moura, M. G. Almeida, *Electrochem. Commun.*, 2007, **9**, 2240; (b) K. Calfuman, M. J. Aguirre, P. Canete-Rosales, S. Bollo, R. Llusar, M. Isaacs, *Electrochim. Acta*, 2011, **56**, 8484.

39 C. Rocchiccioli-Deltcheff, M. Fournier, R. Franck, R. Thouvenot, *Inorg. Chem*. 1983, **22**, 207-216.

40 A. Aupoix, B. Pégot G. Vo-Thanh, *Tetrahedron*, 2010, **66**, 1352.

41 (a) I. Dinarès, C. Garcia de Miguel, N. Mesquida, E. Alcalde, *Green Chem.*, 2009, **11**, 1507; (b) See web site: http://www.il-eco.uft.uni-bremen.de.

42 B. Keita, L. Nadjo, *J. Electroanal. Chem. Inter. Electrochem.*, 1988, **243**, 87.

43 I.-M. Mbomekallé, X. Lopez, J. M. Poblet, F. Sécheresse, B. Keita, L. Nadjo, *Inorg.Chem.*, 2010, **49**, 7001.

44 I. Pezron, M. Djabourov, J. Leblond, *Polymer*, 1991, **32**, 3201.

45 A. Veis, *Adv.Coll. Interface Sci.*, 2011, **167**, 2.

46 (a) M. Petkovic, K. R. Seddon,L. P. N. Rebelo, C. Silva Pereira, *Chem. Soc. Rev.*, 2011, **40**, 1383; (b) M. Opallo, A. Lesniewski, *J. Electroanal. Chem.*, 2011, **656**, 2; (c) M. J. A. Shiddiky, A. A. J. Torriero, *Biosens. Bioelectron.*, 2011, **26**, 1775; (d) K. Fujita, K. Murata, M. Masuda, N. Nakamura, H. Ohno, *RSC Adv.*, 2012, **2**, 4018.

47 A. P. Brown, F. C. Anson, *Anal. Chem.*, 1977, **49**, 1589.

48 F. M. Fernandes, I. Manjubala, E. Ruiz-Hitzky, *Phys. Chem. Chem. Phys.*, 2011, **13**, 4901.

49 S. Dong , X. Xi, M. Tian, *J. Electroanal. Chem.*, 1995, **385**, 227.

50 J. Mocak, A. M. Bond, S. Mitchell, G. Scollary, *Pure Appl. Chem.*, 1997, **69**, 297.

51 (a) E. Ruiz-Hitzky, P. Aranda, M. Darder, M. Ogawa, *Chem. Soc. Rev.*, 2011, **40**, 801; (b) N. Steunou, C. Mousty, O. Durupthy, C. Roux, G. Laurent, C. Simonnet-Jegat, J. Vigneron, A. Etcheberry,C. Bonhomme, J. Livage, T. Coradin, *J. Mater. Chem.*, 2012, **22**, 15291; (c) M. Jaber, F. Ribot, L. Binet,V. Briois, S. Cassaignon, K. J. Rao, J. Livage, N. Steunou, *J. Phys. Chem. C.*, 2012, **116**, 25126.

52 (a) I. Sorribes, G. Wienhöfer, C. Vicent, K. Junge, R. Llusar, M. Beller, *Angew. Chem. Int. Ed.*, 2012, **51**, 7794 ; (b) I. Sorribes, R. Llusar, C. Vicent, *Eur. J. Inorg. Chem.*, 2013, **9**, 1418.

53 (a) X. Huang, M. Li, D. C. Green, D. S. Williams, A. J. Patil, S. Mann, *Nature Comm.*, 2013, **4**, 2239; (b) A. J. Dzieciol, S. Mann, *Chem. Soc. Rev.*, 2012, **41**, 79.